Tunable Charge Transport Using Supramolecular Self-Assembly of Nanostructured Crystalline Block Copolymers

Sven Huettner,[†,‡] Michael Sommer,[‡] Justin Hodgkiss,[¶,†] Peter Kohn,[#,§] Thomas Thurn-Albrecht,[§] Richard H. Friend,[†] Ullrich Steiner,[†] and Mukundan Thelakkat[‡,*]

[†]Cavendish Laboratory, University of Cambridge, United Kingdom, [‡]Applied Functional Polymers, University of Bayreuth, Germany, and [§]Experimentelle Polymerphysik, University of Halle-Wittenberg, Germany. [¶]Present address: MacDiarmid Institute for Advanced Materials and Nanotechnology, School of Chemical and Physical Sciences, Victoria University of Wellington, New Zealand. [#]Present address: Cavendish Laboratory, University of Cambridge, United Kingdom.

ABSTRACT Electronically functionalized block copolymers, combining covalently linked p-type and n-type blocks, show switching behavior of charge transport in organic field effect transistors (OFETs). The electronically active subunits self-assemble into continuous microdomains in a nanoscale regime, thereby forming percolation channels for holes or electrons or both depending on the composition and processing conditions. Here, we establish a charge transport−morphology relation for donor−acceptor block copolymers with two crystalline blocks. The n-type and p-type blocks self-assemble into two-dimensional lattices of $\pi-\pi$ stacks and main chain polymer lamellae, respectively, over a broad composition range. Controlling the crystallization preferences of the two blocks by thermal annealing allows controlling the OFET polarity. Depending on the block ratio, the charge transport can be tuned from p-type to n-type or p-type to ambipolar, respectively. The impact of nanostructured phase separation is further delineated by X-ray diffraction, time-resolved spectroscopy, and scanning electron microscopy studies.

KEYWORDS: charge transport · OFET · donor−acceptor block copolymer · self-assembly · ambipolar · conjugated polymer

Block copolymers will play a major role in many nanotechnology applications because of their scope for well-defined 3-dimensional self-assembly on the nanometer scale.[1] In the simplest case, diblock copolymers consist of two covalently linked polymers. Predictable self-assembled nanostructures result from the tendency of the two blocks to phase separate while remaining attached to each other. The self-assembling properties of block copolymers have inspired widespread application especially in thin film technology such as nanostructured templates.[2,3]

Complementary circuits involving coupled p- and n-type transistors form the basis of efficient logic circuits,[4] which has proven their success in inorganic complementary metal-oxide semiconductor (CMOS) technology. The development of complementary circuitry in organic electronics is an inevitable step for the future of organic circuitry, and different approaches have been demonstrated: Circuitry based on ambipolar organic semiconductors have previously been demonstrated by employing a combination of high- and low work-function metal electrodes in order to achieve dual charge injection into a single semiconductor.[5] Alternatively, a combination of n-type and p-type materials can support dual charge transport using electrodes of a single metal. In analogy with bulk heterojunction solar cells, ambipolar organic field-effect transistor (OFET) devices have been fabricated by coevaporation of small molecules or solution processing a mixture of n-type and p-type polymers.[6,7] In polymer blends, the morphology plays a crucial role in determining the device properties due to the requirement for each electronic component to contact the source and drain electrodes and form sufficient percolation paths for each of the charge carriers. The blend morphology is typically optimized through processing conditions—by adjusting the blend ratio, solvents, or annealing conditions. However, the resulting blend morphologies are nonequilibrium structures that are kinetically trapped during the phase separation process. Additionally, the electronic functionality of a given conjugated material in a blend is often linked to its crystallinity, which is difficult to influence within the constraints of nonequilibrium, kinetically trapped structures.

Another strategy is to combine the functional molecular donor (D) and acceptor (A) units in one macromolecule, either as an alternating copolymer $-[DA]_n-$ or in a

* Address correspondence to mukundan.thelakkat@uni-bayreuth.de.

Received for review September 28, 2010 and accepted April 18, 2011.

Published online April 18, 2011
10.1021/nn200647d

a

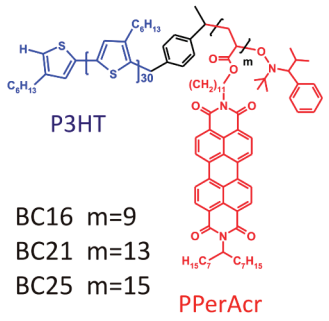

compound	M_n [kg/mol] polydispersity	wt.-% PPerAcr	PPerAcr		P3HT	
			a, b, γ [nm]	c [nm]	a [nm]	b, c [nm]
PPerAcr	23 / 1.71	100	a=3.086 b=2.196 γ=81.2°	0.354	-	-
P3HT	8.9 / 1.12	0	-	-	1.754	0.766
BC 16	16.1 / 1.25	55.7	a=3.078 b=2.206 γ=80.9°	0.365	1.798	0.766
BC 21	20.6 / 1.31	73.7	a=2.987 b=2.096 γ=79.5°	0.365	1.791	0.768
BC 25	24.8 / 1.53	81.4	a=2.988 b=2.105 γ=79.5°	0.363	1.785	0.764

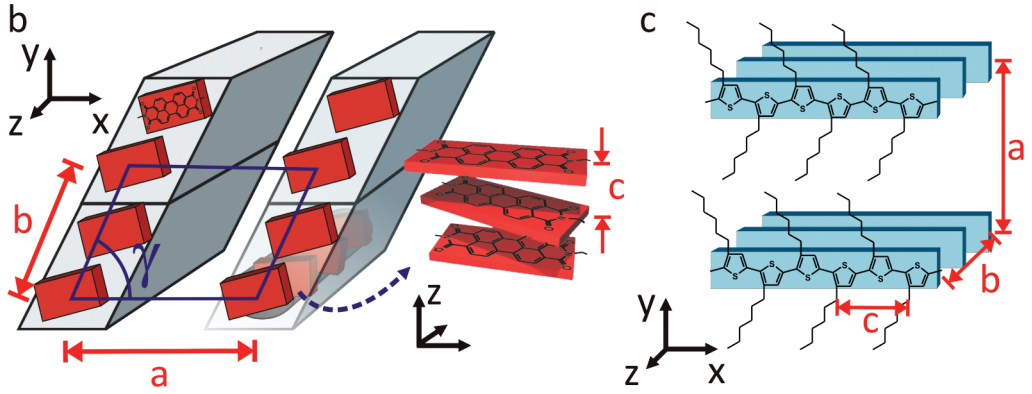

Figure 1. (a) Molecular structure of the block copolymer P3HT-b-PPerAcr. The table shows the properties of the homopolymers and block copolymers together with the unit cell dimensions (at T = 90 °C). Sketch of the crystalline structure of PPerAcr (b) and P3HT (c).

diblock copolymer with covalently bound segments $[D]_n$−block−$[A]_m$. $[DA]_n$ conjugated polymers with a low bandgap have been synthesized. These materials exhibit an intrinsically ambipolar charge transport.[8,9] $[D]_n$−block−$[A]_m$ copolymers consisting of separate, covalently linked D and A polymer chains can self-assemble into bicontinuous domains for p-type and n-type charge transport. They bridge the gap between $[DA]_n$ materials[10,11] and donor−acceptor blends. In these block copolymers, polymer crystallinity of each domain, which is important for the charge transport, can be combined with a well-defined interconnectivity of both domains.

Equilibrium nanostructured morphologies of diblock copolymers with two amorphous blocks are well-known,[12] but morphologies in block copolymers with rodlike units[13] or crystallizable blocks are much more complicated to predict.[14−16] Nevertheless, the covalent bond between the donor- and acceptor subchains always ensures nanoscale heterogeneity and, together with the control of crystallization preferences, offers potential for new device processing possibilities.

Here we report on the first OFETs realized with fully functionalized diblock copolymers and demonstrate the relationship between composition, crystallinity, and charge transport. More importantly, the charge transport in the OFETs can be set—depending on the block ratios of the material—either from p-type to ambipolar or from p-type to n-type device characteristics in one single material depending on the processing conditions. This potentially opens new possibilities for the design of complementary electronic elements by simple solution processing of a single component. We have studied a series of diblock copolymers, BC16, BC21, and BC25, comprising regioregular poly(hexylthiophene) (P3HT) and poly(perylene bisimide acrylate) (PPerAcr) subchains in different volume ratios.[17] The chemical structure, the overall molecular weight M_n, the polydispersity (PDI), and the composition are given in Figure 1.

P3HT is a ubiquitous hole transporter (donor material) that is among the most effective polymers in organic photovoltaics and OFETs, owing to field effect hole mobilities up to 0.1 $cm^2/(V\ s)$.[18,19] The crystalline structure of P3HT is well-known[20,21] (Figure 1c). Perylene bisimides (PBIs) are one class of n-type materials (acceptor material) that combine promising electronic properties with good air stability. Low molecular weight PBIs have shown electron mobilities as large as 2.1 $cm^2/(V\ s)$ in evaporated thin films.[22,23] Furthermore, the attachment of side chains at the imide groups renders them soluble in common organic solvents and an alteration of the intermolecular packing without changing the delocalized π-electron

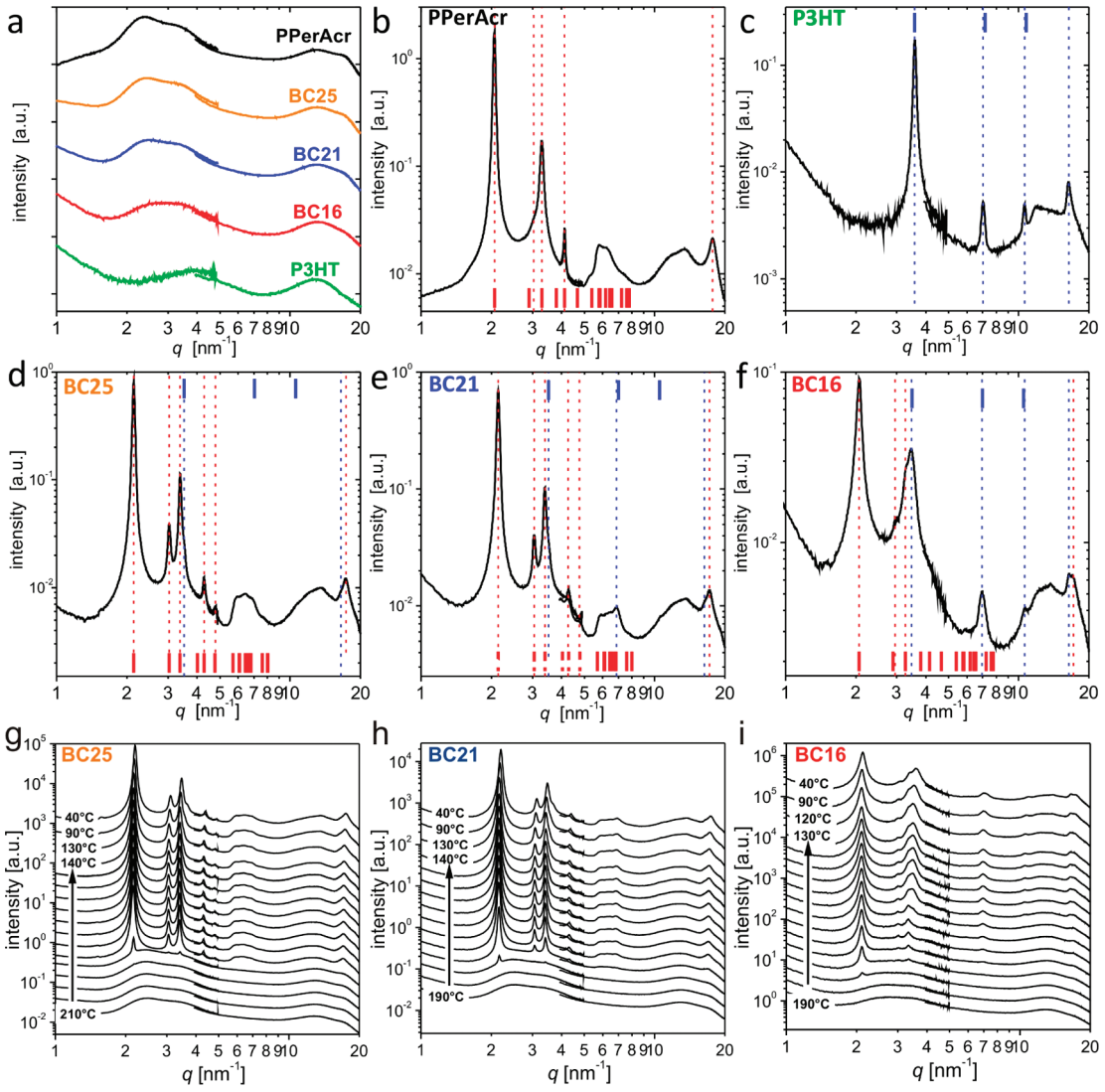

Figure 2. Radially averaged SAXS/WAXS patterns of bulk samples. (a) At high temperatures $T = 210$ °C all the samples are molten and do not show any Bragg-reflections; the curves are offset for clarity. During cooling the PPerAcr- and P3HT-parts of the diblock copolymers crystallize and Bragg reflections appear; (b−f) the corresponding patterns at $T = 90$ °C for the different samples as indicated in the graphs. The dashed lines correspond to peak positions obtained by fitting Lorentz functions to the data: red, PPerAcr; blue, P3HT. The red (PPerAcr) and blue (P3HT) bars correspond to expected peak positions for the lattice parameters given in Figure 1a. (g−i) the SAXS/WAXS pattern evolves when cooled from melt at a rate of 10 K/min. The PPerAcr has the lower melting temperature compared to P3HT, however recrystallizes first, disturbing the formation of long-range ordered P3HT. This effect becomes more pronounced with increasing PPerAcr content.

system within the PBI core.[24] Alkyl substituents can be used to induce the formation of one-dimensional columnar PBI aggregates.[25,26] We have recently reported a polymerized form of this PBI (PPerAcr) that exhibits electron mobilities of 10^{-3} cm^2/(V s) and good electron injection from gold electrodes.[27] The latter fact is important since the higher LUMO levels of other n-type materials usually necessitate low work function metals such as aluminum, calcium, or magnesium as electrodes.

RESULTS AND DISCUSSION

Before describing the OFET properties in thin film devices, we first present some fundamental X-ray characterization of the nanostructured bulk material. The relative composition of the block copolymers barely affects the crystal structure (as ascertained by peak positions), while the relative degree of crystallinity is strongly influenced (as ascertained by peak intensities). This is an important property which will influence the charge transport, that is, the formation of nanoscopic percolation paths. We studied the temperature-dependent structure formation in the homopolymers and the block copolymers using X-ray scattering by slowly cooling from the molten state (Figure 2a). The PPerAcr homopolymer (Figure 2b, schematic in Figure 1b) shows a crystallization of the PBI cores into stacks with a π-stacking distance of $c = 0.354$ nm (X-ray reflection at $q = 17.75$ nm^{-1}).

These stacks arrange into 2-d lattices (Figure 1b). We find good agreement of the observed Bragg reflections

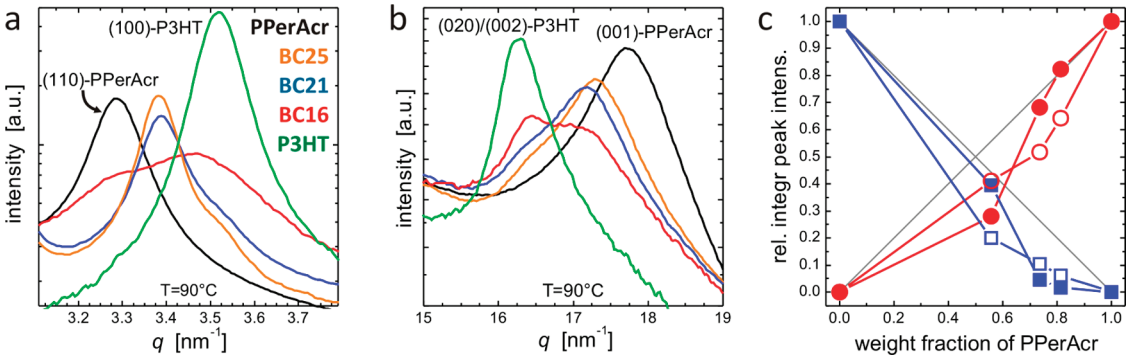

Figure 3. (a) Overlap of the (110) PPerAcr reflection and the (100) P3HT reflection. For BC21 and BC25 the (110) PPerAcr reflection is slightly shifted due to a little different unit cell and the (100) P3HT reflection is still visible as a shoulder at ~3.5 nm^{-1}. (b) Change of the overlapping (020)/(002)-reflection of the P3HT-crystallites and the (001)-reflection of PPerAcr with copolymer composition (green, P3HT; red, BC16, blue, BC 21; yellow, BC 25; and black, PPerAcr). (c) Integrated Bragg-reflection intensities normalized to the homopolymer values as a function of PPerAcr-content. Open symbols correspond to (020)/(002)-reflection of P3HT (blue squares) and (001)-reflection of PPerAcr (red circles) and filled symbols represent the integrated intensities of the (100)-reflection of P3HT (squares) and PPerAcr (circles), respectively.

(red dashed lines in Figure 2b) with the reflections expected for a 2-d oblique lattice with parameters a = 3.086 nm, b = 2.196 nm, and γ = 81.2° (red bars in Figure 2b). The number of PBI cores per unit cell can be estimated by assuming that the overall density is not much smaller than 1 g/cm^3. Thus a value for the density of 1.14 g/cm^3 is obtained by dividing the mass of two PPerAcr monomers (molar mass per monomer: 825 g/mol) by the volume of the unit cell ($V = abc \sin\gamma$).[28] Because there are 2 PBIs per unit cell, the comparison of the lattice parameter b with the molecular dimension of the PBI core leads us to suggest a lamellar packing as shown in Figure 1. Consistent with this arrangement, the (010) reflection is strongly suppressed by the form factor of the unit cell, and only a weak shoulder is visible in Figure 2b at 3 nm^{-1}. For the block copolymers the unit cell structure slightly changes leading to a clearly visible (010) reflection mainly attributed to the slight change in γ.

Figure 2c shows evidence for the crystallinity of P3HT. The first three reflections correspond to the (h00)-reflections for h = 1, 2, 3 with a = 1.754 nm (*cf.* Figure 1b). The reflection at q = 16.41 nm^{-1} is a combined reflection of the inter- and intrachain stacking (b- and c-direction) with the corresponding Miller indices (020)/(002). The values for lattice parameters a and $b = c$ (determined at T = 90 °C) are in close agreement with the lamellar packing reported in the literature.[29] Having thus identified the signatures of the PPerAcr and P3HT homopolymer lattices, we have studied the series of asymmetric block copolymers which have PPerAcr-weight fractions of 55.7% (BC16), 73.7% (BC21), and 81.4% (BC25). The molecular weight of the P3HT-block was 8.9 kg/mol in all cases. After crystallization from the melt (same thermal treatment as for the homopolymers), the scattering patterns in Figure 2d–f closely resemble a combination of the Bragg reflections in Figure 2b,c, though small changes in the unit cell parameters were observable (Figure 1a). The signature of both crystal structures in these patterns (red and blue dashed lines and Figure 3) provides clear evidence that phase separation occurs in all three block copolymers. The covalent linkage of both blocks ensures a nanoscopic phase separation. Indeed probing the charge generation dynamics by ultrafast spectroscopy as shown below, the estimated domain sizes range below 10 nm which is consistent with the molecular dimensions of the blocks (estimated contour length of the P3HT block of approximately 11.6 nm). (Additional scanning electron microscopy images on the nanoscopic phase separation are given in the Supporting Information.)

The separated crystals of donor and acceptor units demonstrate the potential applicability of these block copolymers in devices. Figure 3 panels a and b show compilations the five polymers of (a) the (110) PPerAcr reflection and the (110) P3HT reflection and (b) the q-range where the (020)/(002)-reflection of the P3HT-crystals and the (001)-reflection and the PPerAcr-crystals appear. Though the P3HT reflections in Figure 3a,b for higher PPerAcr content appeared only as weak shoulders, we tried to estimate the change in P3HT crystallinity as a function of PPerAcr content by considering the respective peak intensities (Figure 3c). At higher PPerAcr content the P3HT crystallinity seemed to be lower than expected from a linear scaling. This indicates that part of the P3HT chains were not able to crystallize and frustrated by PPerAcr crystallization, an observation which is also consistent with optical spectroscopy (*vide infra*). The corresponding crystallization kinetics can be followed in Figure 2g–i. PPerAcr melts first upon heating, but also recrystallizes first upon cooling compared to the P3HT block.

The competing crystallization behavior can be used to adjust the charge carrier properties in an OFET device. The polymer was spin-coated from chloroform solution onto bottom gate, bottom contact OFET substrates. Despite the higher PPerAcr

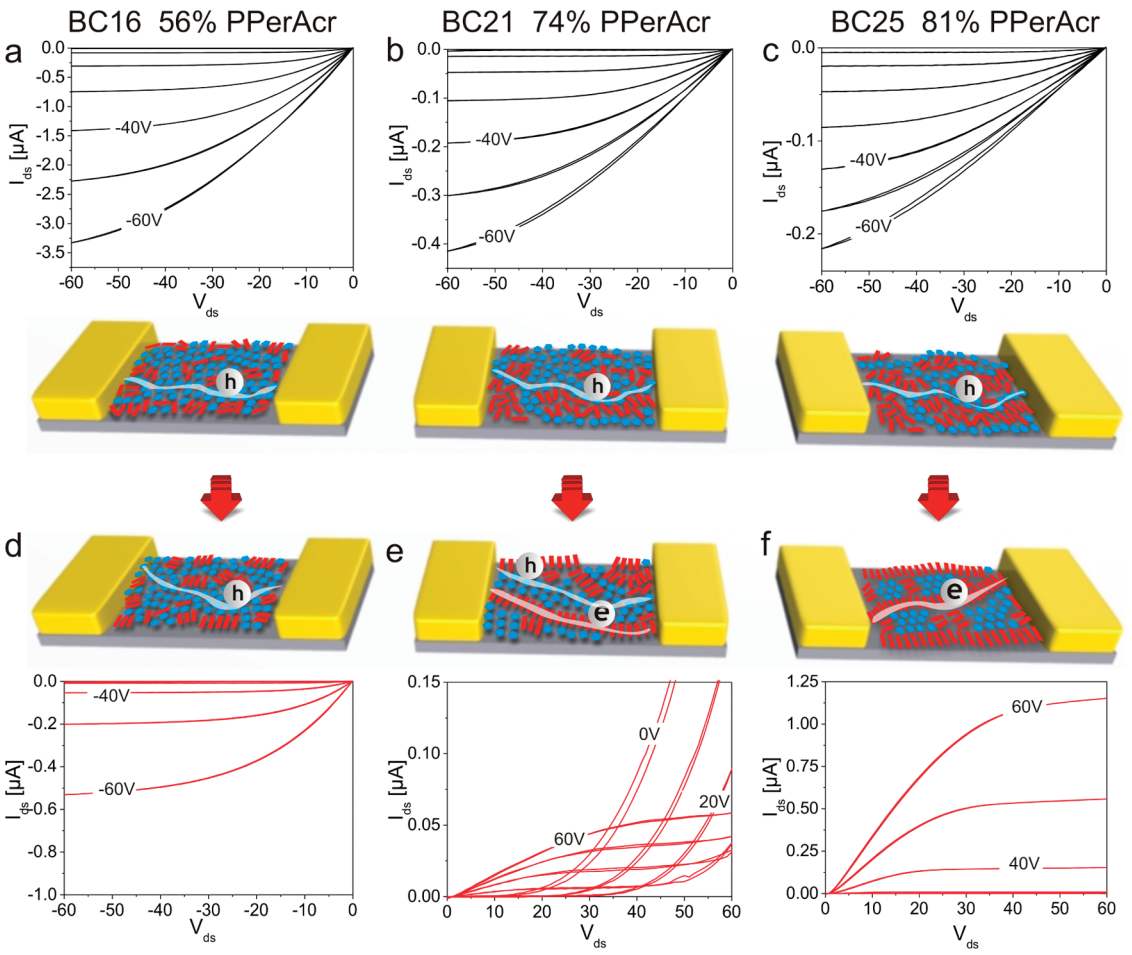

Figure 4. (a–f) Output characteristics of OFETS made from BC16, BC21, BC25 before annealing (a–c, black curves) and after annealing (d–f, red curves). The gate voltage V_g was varied from 0 to 60 V in steps of 10 V. Before annealing all transistors show unipolar p-type character, whereas after annealing ambipolar transport was observed for BC21 and unipolar n-type transport for BC25. Schematics of the thermally induced structure–function transition in block copolymer OFETs are shown in between the output graphs. Before annealing (upper sketch) P3HT forms hole percolation paths between the source and drain electrode. After cooling from melt (lower sketch), n-type percolation paths dominate, and the transistor switches to ambipolar or n-type behavior.

weight fraction compared to the P3HT content, we found that all block copolymers exhibited p-type character after spin coating. Figure 4 shows the OFET output characteristics for devices made with the three copolymers. All as-spun films (Figure 4a–c) show typical unipolar hole transport, even the block copolymer with a PPerAcr weight content of 81% PPerAcr. The overall drain–source current I_{ds} decreases slightly with increasing PPerAcr content presumably indicating an increasing lateral disruption of hole conducting channels. The contact resistance was low in all cases, as indicated by the linear raise of drain source current I_{ds} for applied voltages $V_{ds} < 0$. Figure 5 panels a–c (black lines) show the transfer characteristics measured for these p-type devices. The measurements indicate hole injection from the drain electrode, leading to decreasing output characteristics with increasing gate voltages. Hole mobilities of around 10^{-5} $cm^2/(V\ s)$ were extracted in the saturation regime.

The P3HT homopolymer can exhibit hole mobilities which are orders of magnitude higher; however, the low molecular weight fraction of the block strongly limits the maximal achievable mobilities.[30] Electron injection was observed in some of the more PPerAcr rich devices only at very high drain–source voltages (data not shown). The predominance of p-type transport indicates that only the P3HT component forms sufficiently interconnected domains to support the creation of a channel from source to drain in spin-cast films. We attribute this to the fact that the thiophene units are part of a conjugated polymer chain that supports both interchain and intrachain charge transport,[19,31] thus providing more interconnected percolation paths for holes. On the other hand, the formation of electron conduction pathways in PPerAcr is subject to intermolecular π-orbital overlap of the tethered PBI moieties. Additionally, the weight percentage of the PBI block does not resemble the real content of PBI electronic moieties due to high dilution

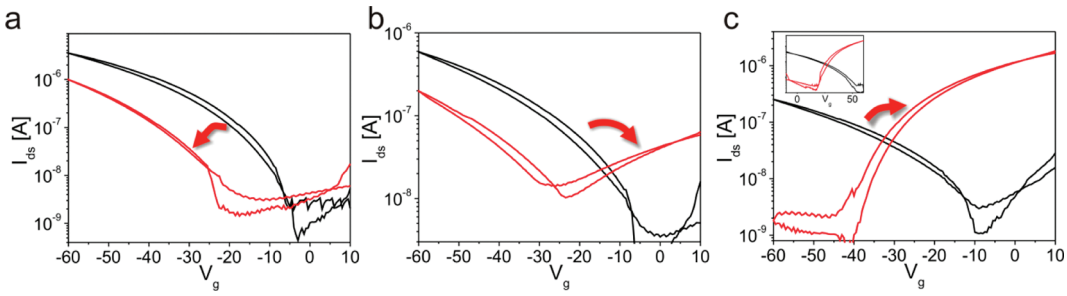

Figure 5. Transfer characteristics of the block copolymer transistors measured in p-type configuration at $V_{ds} = -60$ V. The black and red curves show the as-spun and annealed devices, respectively. (a) BC16 remains unipolar p-type, (b) BC21 shows ambipolar properties, and (c) BC25 switches to unipolar n-type after annealing. The inset of (c) shows the transfer characteristic of BC25 measured in n-type configuration. (For additional output and transfer characteristics see Supporting Information Figure S1, Figure S2).

caused by substituents, which are necessary for solubility. The percolation path formation is also influenced by rapid drying during the spin-coat process, which freezes-in nonequilibrium structures.

After a thermal annealing step at 225 °C (above the melting temperature of both components, Figure 2a) for 15 min and cooling down at 10 K/min (similar to the X-ray studies), the OFET properties changed drastically depending on the block copolymer composition. After being annealed (Figure 4d–f), BC16 retains p-type behavior but with slightly reduced currents and an increased threshold voltage for hole accumulation V_{ThH}. In the case of BC21 (Figure 4b,e), an ambipolar character was found, with both holes and electrons accumulating in the channel. The most significant transition occurred for BC25, the block copolymer containing the highest PPerAcr content (Figure 4c,f). Upon thermal annealing, the polarity of the BC25 device switched entirely from p-type to n-type transport.

Figure 5a–c shows the transistor transfer characteristics before and after annealing. The extracted hole mobilities from the OFETs in saturation before annealing account for 10^{-5} cm^2/(V s) . The P3HT hole mobilities are relatively small, which is related to the short P3HT block length.[32] The electron mobilities for the annealed BC21 and BC25 are around 10^{-5} cm^2/(V s), which is 2 orders of magnitude lower than the mobility of the pristine homopolymer.[27] The ambipolar character of the annealed BC21 transistor is clearly evident in its characteristic V-shaped transfer characteristic (Figure 5b), caused by the injection of electrons *via* the drain electrode, while measuring in p-type configuration (see Supporting Information). Figure 5c shows the complete switch from a p-type to an n-type behavior of the device upon annealing and only a marginally small injection of holes is noticeable.

We identify two main reasons for the switching in transistor characteristics upon annealing. First, the fact that both p- and n-type polymer segments are covalently connected means that the scope of the phase separation is constrained to the nanometer length scale. Thus, both polymer segments are in close proximity to the gate dielectric interface and are potentially able to form field-effect charge carrier channels. The second reason is the interplay of the crystallization behavior of the two polymers—the main chain crystallinity of P3HT and the side chain crystallinity of PPerAcr. Thermal annealing enables the PBI units to rearrange sufficiently into $\pi-\pi$ stacks building up the 2-d lattice causing enhanced intramolecular electronic coupling. However, the crystallinity of PPerAcr apparently improves at the expense of the crystallinity (see discussion of Figure 3c above) and connectivity of P3HT domains. In the case of the BC21, the interconnectivity and crystallinity of both components was sufficiently high that both electron and hole percolation paths could form, leading to an ambipolar device. The OFET properties of BC25 were dominated by the formation of percolating PPerAcr stacks after annealing. The X-ray analysis carried out on bulk samples of the block copolymers support this observed evolution of the crystalline domains during annealing (Figure 2g–i).

An alternative explanation of the change in transistor characteristics upon annealing involves the possible build-up of a PPerAcr wetting layer on the gate, displacing the P3HT domains further into the bulk of the film. To test this hypothesis, X-ray photoelectron spectra (XPS) of the bottom surface (in contact with the gate) of the block copolymer films were carried out. No significant differences between the as-spun and the annealed samples were observed. On the other hand, a comparison of the XPS-spectra of the homopolymers shows significant differences in the relative signals of N and O (present only in PPerAcr) and S (present only in P3HT, Supporting Information Figure S4).

Directly resolving the morphology at the gate oxide interface is not simple as the domains are on the edge or beyond the resolution of standard scanning electron microscopy or scanning force microscopy. In the latter case, for example, the stiffness of both blocks strongly limits a possible phase contrast. Only extensive solvent vapor annealing of the samples provides a sufficient contrast in SEM (see Supporting Information Figure S5).

To substantiate the above findings and to obtain an indirect access to the nanoscopic structure of the material, we also employed several complementary spectroscopic methods to investigate the evolution of crystallinity in thin films. The overlap of the π-orbitals within crystals of conjugated materials causes morphology-dependent changes in transition dipole moments and therefore in optical absorption and emission spectra. The degree of aggregation can be assessed by comparing the relative intensities of vibronic bands. For PBI, the relative intensities of vibronic bands at 490 and 540 nm can be considered to estimate the effect of aggregation.[33] Figure 6a shows the absorption spectra of the two homopolymers P3HT and PPerAcr after spincoating and after thermal annealing for 10 min at 225 °C followed by cooling down at 10 K/min. Absorption spectroscopy confirms the favorable aggregation of PBI moieties after thermal annealing. The main spectral changes of PPerAcr after thermal annealing are the suppression of higher energy absorption combined with the emergence of a low energy shoulder (see change in relative intensities of the vibronic bands). The improved PBI aggregation decreases the oscillator strength of transitions to higher vibronic levels, whereas the new low energy features are attributed to charge transfer states and mixed Frenkel-charge transfer states.[34] A general feature of crystalline P3HT films is the strength of the 0−0 vibronic band at 610 nm which is indicative of extended planarized chains.[35,36] The P3HT homopolymer shows marginal enhancement of this vibronic band for the annealed film compared to the as-spun film. Figure 6b shows the absorption spectra of the block copolymers. For the as-prepared sample (solid lines), little difference is seen among the three block copolymers. The absorption spectra are broadly described as a weighted average of the homopolymer spectra according to their respective weight ratios. However, the suppression of the P3HT 0−0 vibronic feature in the block copolymers is clear evidence that the presence of the PPerAcr block disrupts the full crystallization of P3HT. Thermal annealing induces similar spectral changes in the absorption spectra of block copolymers as observed in the constituent homopolymers (Figure 6a). The suppression of higher energy absorption features is accompanied by the growth of lower energy absorption peaks as the crystallinity of both blocks improves. The spectral shifts on annealing are clearly dominated by the increased crystallization of the PPerAcr component, explaining the observed switching behavior of polymers with the highest content of PPerAcr.

In addition to absorption spectroscopy which provides a picture of the overall changes in crystallinity throughout the films, transient absorption (TA) spectroscopy was employed to extract information about nanoscale morphological changes in the vicinity of interfaces. A detailed discussion of the TA data is provided elsewhere.[38] As is typical for nanostructured donor−acceptor systems, photoexcitation results in the formation of interfacial charge pairs, with holes and electrons in the P3HT and PPerAcr phases, respectively. The information gained by TA spectroscopy is based upon spectral signatures of crystallinity for excitons (the primary excitation, formed throughout the film) compared with charge pairs (formed at later times, localized near donor−acceptor interfaces).

Figure 6d−f shows the effect of annealing on excitonic spectra (recorded at $\tau \approx 0.1-1$ ps delay after the excitation pulse) and interfacial charge spectra ($\tau \approx 1-1.9$ ns) for the block copolymers. At $\tau \approx 0.1-1$ ps delay (red and orange curves), the spectra largely represent a weighted average of excitonic spectra of both homopolymers, which are shown in Figure 6c. At $\lambda < 620$ nm, the positive $\Delta T/T$ signal is dominated by ground-state bleaching (GSB) of the P3HT chromophore and corresponds to the ground state absorption spectrum. Analogous to the ground state absorption spectra, bleaching of the 0−0 peaks at 610 nm is suppressed in the as-spun films (red curves, Figure 6d−f). We are able to assign the $\tau \approx 1-1.9$ ns TA spectra to interfacial charge pairs based on the strong photovoltaic response of the material and the persistence of the spectra on time scales that far exceed exciton lifetimes.[38]

The TA spectra shown beyond $\tau \approx 1-1.9$ ns in Figure 6d−f exhibit photoinduced absorption at $\lambda > 630$ nm (attributed to charges in both phases) and ground-state bleaching at $\lambda < 630$ nm (largely corresponding to the P3HT chromophore). As was the case for exciton TA spectra, the vibronic structure of the P3HT-based bleach signal can be interpreted on the basis of the crystallinity of polymer chains occupied by excitations. The close resemblance of the charge pair spectra obtained before (blue curves) and after (green curves) thermal annealing, and the suppression of GSB intensity in the 610 nm region with higher PPerAcr content clearly show that P3HT is increasingly disordered at the interfaces where charge pairs are detected.

Since the time scale of exciton diffusion limited charge generation (*i.e.*, formation of charge transfer states) is directly related to the size of domains, we can extract nanometer-scale morphological parameters on a length scale that is not resolved by electron microscopy.[39,40] The population of charge pairs peaks within just 2 ps, as ascertained from the growth of the photoinduced absorption at 700 nm. (In addition to charge pairs, PPerAcr-based excitons also exhibit absorption at 700 nm. However, the growth of absorption at 700 nm cannot be attributed to energy transfer from P3HT to PPerAcr because the P3HT-based groundstate bleach is retained on this time scale.)[38] The short time scale reflects the close proximity of most P3HT regions

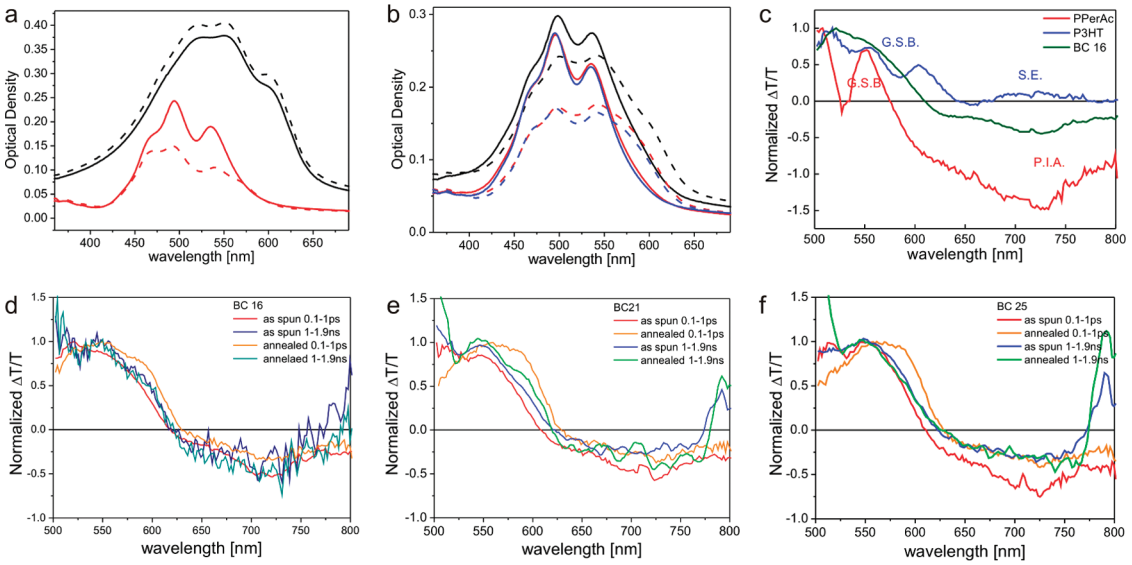

Figure 6. (a and b) UV−vis spectra of the as spun (solid line) and annealed (broken line) film: (a) the homopolymers P3HT (black) and PPerAcr (red); (b) the block copolymer samples with BC16 (black), BC21 (red), BC25 (blue). (c−f) Transient absorption spectroscopy data: (c) representative TA spectra of the homopolymers taken within the first picosecond after excitation. A positive change in the transmission as a result of photoexcitation ($\Delta T/T > 0$) indicates a groundstate bleach (GSB) or a stimulated emission (SE), whereas a negative change indicates photo induced absorption (PIA). The broad PIA peaked at 730 nm is associated with excitons in PPerAcr, consistent with other photophysical studies of perylene diimides.[37] (d−f) Comparison of the TA spectra for block copolymer BC16 (d), BC21 (e), and BC25 (f) right before and after annealing on subpicosecond and nanosecond time scales. Thermal annealing results in some ordering of P3HT, as evident by the enhanced GSB intensity in the 0−0 vibronic band at 610 nm for the subpicosecond exciton spectra; however, ordering is disrupted at the interfaces with the PPerAcr block, as evident from the invariance of interfacial charge pair spectra recorded at 1−1.9 ns (for the respective kinetic plots see Supporting Information Figure S6).

to an interface less than 10 nm. Thus, after spincoating the domains are considerably smaller than those expected for thermodynamic equilibrium structures (*e.g.,* obtained after extensive annealing).

The charge transfer kinetics for all samples remain largely unchanged after 15 min thermal annealing. This clearly indicates that the domain sizes do not change considerably during the device annealing procedure. This is also consistent with the complete quenching of emissive P3HT excitons in photoluminescence measurements.[38] Constistent with the bulk crystallinity measurements (Figure 3c), an increasing content of PPerAcr influences the subsequent crystallization of P3HT. The observation of reduced P3HT crystallinity at the interfaces with PPerAcr *via* TA spectra of interfacial charge pairs illustrates the conflicting crystallinity demands of both components manifested at their interface. OFET measurements show that a high content of PPerAcr is sufficient to severely disrupt the connectivity of P3HT networks hence to suppress p-type transport.

CONCLUSION

We have demonstrated a series of double-crystalline block copolymers that comprise a hole transporting P3HT block (p-type) and an electron transporting PPerAcr block (n-type). The n-type block self-aggregates into a nanoscopic two-dimensional lattice comprising PPerAcr stacks, and the p-type block consisting of P3HT crystallizes in its well-known lattice. The interplay of the crystallinity and the block sizes determine the formation of percolating paths that lead to either p-type, n-type or ambipolar behavior. Directly after solution processing, which results in a nonequilibrium morphology, only the P3HT phase provides sufficiently interconnected pathways. This is the case for all the block copolymers including BC25, in which the P3HT weight content is only 19%. A thermal annealing step enhances the formation of crystalline PPerAcr domains that favor n-type transport. However, PPerAcr crystallization is shown to impede the formation of interconnected P3HT pathways. Depending on the composition of the block copolymer, the devices switched from unipolar hole transport to ambipolar or unipolar electron transport in a single material.

These results demonstrate the versatility of fully functionalized block copolymers as a new class of materials for the application in organic thin film transistors. Broadening the range of supramolecular structures of P3HT-*b*-PPerAcr is feasible by different annealing methods such as solvent annealing,[41] or by further changing the block size. Spatially resolved thermal annealing by laser heating is under current investigation as a means of selectively defining the polarity of transistors within an array on a substrate in a postprocessing step. The covalent linkage of the two blocks preserves the nanoscopic structure after extensive annealing procedures and therefore the block

copolymers are expected to provide robust systems when subject to different annealing parameters during device fabrication. We believe that these results will inspire further efforts toward complementary logic electronic applications based on supramolecular assembly of materials with multiple electronic functionalities.

EXPERIMENTAL SECTION

The polymers were dissolved in water-free chloroform 0.7−1 wt % solution and spincast on the respective substrates at 2000 rpm. For the OFETs we used lithographically prepatterned substrates. The drain and source contacts were interdigitating gold electrodes with gate lengths of 10 μm and gate widths of 20 mm. Highly n-doped silicon wafer with a 300 nm thick silicon oxide layer was used as the gate dielectric. Prior to spin-coating, the substrates were solvent and plasma cleaned and then subsequently silanized by HMDS vapor for approximately 3 h. The transport properties of the transistors were measured with a HP4155A or HP4155B parameter analyzer. All OFET preparation and characterization steps were carried out in a glovebox under nitrogen atmosphere. The charge carrier mobility μ was extracted in the saturation region of the transfer characteristics using $I_d = W/L\ \mu_{sat}C_i(V_g - V_{Th})^2$, where W is the gate width, L is the gate length, C_i is the silicon oxide capacitance, and V_{th} is the threshold voltage.

X-ray diffraction was measured at the ESRF Synchrotron in Grenoble at Beamline ID02. The energy of the X-rays was 12.54 keV. The sample consisted of a polymer powder which was pressed into holes of aluminum discs with holes of 0.8 mm diameter and a thickness of 1 mm. The thermal measurements where carried out at 10 K/min under inert gas atmosphere. Two detectors were used simultaneously to cover a wide q range overlapping at $\sim$1 nm^{-1}. Para-bromo benzoic acid was used to calibrate the detectors. The measurements were corrected by empty cell measurements.

X-ray photoelectron spectra (XPS) of the bottom side of the block copolymer films were obtained. Films were prepared on silicon oxide coated silicon wafers using the same procedure as for the organic field effect transistors. A protective platinum layer was sputtered on top and an epoxy resin was glued to that. The silicon substrate was then removed from the film and the resin by liquid nitrogen, so that the bottom of the polymer film was exposed and could be analyzed by XPS (Perkin-Elmer PHI-5600). The complete delamination of the film was assured by optical investigation of the initial silicon oxide substrates.

For the spectroscopic measurements, the polymers were spin-coated onto spectrosil quartz glass. The UV−vis measurements were carried out with a Hewlett-Packard 8453 diode array spectrometer.

The setup for transient absorption (TA) spectroscopy is described elsewhere.[42−44] Briefly, a 1-kHz train of 60 fs pulses (800 mJ/pulse, λ_0 = 800 nm) is split; a portion used to pump a TOPAS optical parametric amplifier to tune the excitation pulses, and a further portion of the 800-nm beam is used to pump a home-built broadband noncollinear optical parametric amplifier (NOPA)[42] for broadband TA spectra. The probe beam is delayed relative to the excitation beam *via* a mechanical delay stage before overlapping with the excited region of the film. In the spectral measurements, the probe beam is spectrally resolved and digitized for each laser pulse. The excitation beam is chopped at 500 Hz such that the transmission of alternate probe pulses can be compared to obtain the spectrally resolved differential transmission as a result of excitation, and temporal dynamics are compiled by collecting spectra for a range of relative probe delay times (typically $\sim$150 points are distributed from −10 to 2000 ps). Samples were contained in a vacuum chamber ($\sim 10^{-5}$ mbar) during TA measurements.

Acknowledgment. We acknowledge the European Synchrotron Radiation Facility for provision of synchrotron radiation facilities, and we would like to thank M. Stuecky for assistance in using beamline ID02. The authors thank M. Kolle and H. Schoberth for their support during the X-ray measurements. We also thank Prof. Dr. Jürgen Rühe group, IMTEK, Freiburg, for the XPS measurements. We acknowledge the financial support from the European network "PolyFilm" under RTN-6 and the German Research Council (DFG) project SPP 1355. S.H. thanks Universität Bayern e.V. for the financial support in the form of a scholarship of the Bayerische Graduiertenförderung and the Elitenetzwerk Bayern (ENB) for their support. J.M.H. and R.H.F. wish to acknowledge a grant from the U.K. Engineering and Physical Sciences Research Council (EPSRC).

Supporting Information Available: Complete OFET characteristics, thermal data, SEM pictures, and XPS data. This information is available free of charge *via* the Internet at http://pubs.acs.org.

REFERENCES AND NOTES

1. Park, C.; Yoon, J.; Thomas, E. Enabling Nanotechnology with Self Assembled Block Copolymer Patterns. *Polymer* **2003**, *44*, 6725–6760.
2. Tang, C.; Lennon, E.; Fredrickson, G.; Kramer, E.; Hawker, C. Evolution of Block Copolymer Lithography to Highly Ordered Square Arrays. *Science* **2008**, *322*, 429.
3. Park, S.; Lee, D.; Xu, J.; Kim, B.; Hong, S.; Jeong, U.; Xu, T.; Russell, T. Macroscopic 10-Terabit-per-Square-Inch Arrays from Block Copolymers with Lateral Order. *Science* **2009**, *323*, 1030.
4. Crone, B.; Dodabalapur, A.; Lin, Y.; Filas, R.; Bao, Z.; LaDuca, A.; Sarpeshkar, R.; Katz, H.; Li, W. Large-Scale Complementary Integrated Circuits Based on Organic Transistors. *Nature* **2000**, *403*, 521–523.
5. Cornil, J.; Brédas, J.-L.; Zaumseil, J.; Sirringhaus, H. Ambipolar Transport in Organic Conjugated Materials. *Adv. Mater.* **2007**, *19*, 1791–1799.
6. Rost, C.; Karg, S.; Riess, W. Ambipolar Light-Emitting Organic Field-Effect Transistor. *Appl. Phys. Lett.* **2004**, *85*, 1613–1615.
7. Loi, M. A.; Rost-Bietsch, C.; Murgia, M.; Karg, S.; Riess, W.; Muccini, M. Tuning Optoelectronic Properties of Ambipolar Organic Light-Emitting Transistors Using a Bulk-Heterojunction Approach. *Adv. Funct. Mater.* **2007**, *16*, 41–47.
8. Steckler, T. T.; Zhang, X.; Hwang, J.; Honeyager, R.; Ohira, S.; Zhang, X.; Grant, A.; Ellinger, S.; Odom, S.; Sweat, D.; *et al.* A Spray-Processable, Low Bandgap, and Ambipolar Donor−Acceptor Conjugated Polymer. *J. Am. Chem. Soc.* **2009**, *131*, 2824–2826.
9. Kim, F. S.; Huo, X.; Watson, M. D.; Jenekhe, S. A. High-Mobility Ambipolar Transistors and High-Gain Inverters from a Donor−Acceptor Copolymer Semiconductor. *Adv. Mater.* **2009**, *21*, 478–482.
10. Singh, T. B.; Günes, S.; Marjanovic, N.; Sariciftci, N. S.; Menon, R. J. Correlation between Morphology and Ambipolar Transport in Organic Field-Effect Transistors. *Appl. Phys.* **2005**, *97*, 114508.
11. Cravino, A.; Sariciftci, N. Molecules as Bipolar Conductors. *Nat. Mater.* **2003**, *2*, 360–261.
12. Bates, F.; Fredrickson, G. Block Copolymer Thermodynamics: Theory and Experiment. *Annu. Rev. Phys. Chem.* **1990**, *41*, 525–557.
13. Olsen, B. D.; Segalman, R. A. Self-Assembly of Rod−Coil Block Copolymers. *Mater. Sci. Eng.* **2008**, *62*, 37–66.
14. Hamley, I.; Fairclough, J.; Ryan, A.; Bates, F.; Towns-Andrews, E. Crystallization of Nanoscale-Confined Diblock Copolymer Chains. *Polymer* **1996**, *37*, 4425–2249.
15. Nojima, S.; Kato, K.; Yamamoto, S.; Ashida, T. Crystallization of Block Copolymers. 1. Small-Angle X-ray Scattering Study of a ε-Caprolactone-Butadiene Diblock Copolymer. *Macromolecules* **1992**, *25*, 2237–2242.
16. Loo, Y.-L.; Register, R. A.; Ryan, A. J. Modes of Crystallization in Block Copolymer Microdomains: Breakout, Templated, and Confined. *Macromolecules* **2002**, *35*, 2365–2374.

17. Sommer, M.; Lang, A. S.; Thelakkat, M. Crystalline–Crystalline Donor–Acceptor Block Copolymers. *Angew. Chem., Int. Ed.* **2008**, *47*, 7901–7904.
18. Sirringhaus, H.; Brown, P. J.; Friend, R. H.; Nielsen, M. M.; Bechgaard, K.; Langeveld-Voss, B. M. W.; Spiering, A. J. H.; Janssen, R. A. J.; Meijer, E. W.; Herwig, P.; *et al*. Two-Dimensional Charge Transport in Self-Organized, High-Mobility Conjugated Polymers. *Nature* **1999**, *401*, 685.
19. Chang, J.-F.; Sun, B.; Breiby, D. W.; Nielsen, M. M.; Sölling, T. I.; Giles, M.; McCulloch, I.; Sirringhaus, H. Enhanced Mobility of Poly(3-hexylthiophene) Transistors by Spin-Coating from High-Boiling-Point Solvents. *Chem. Mater.* **2004**, *16*, 4772–4778.
20. Hugger, S.; Thomann, R.; Heinzel, T.; Thurn-Albrecht, T. Semicrystalline Morphology in Thin Films of Poly-(3-hexylthiophene). *Colloid Polym. Sci.* **2004**, *282*, 932–938.
21. Wu, Z.; Petzold, A.; Henze, T.; Thurn-Albrecht, T.; Lohwasser, R.; Sommer, M.; Thelakkat, M. Semicrystalline Morphology in Thin Films of Poly(3-hexylthiophene). *Macromolecules* **2010**, *43*, 4646–4653.
22. Chesterfield, R. J.; McKeen, J. C.; Newman, C. R.; Ewbank, P. C.; daSilva Filho, D. A.; Brédas, J.-L.; Miller, L. L.; Mann, K. R.; Frisbie, C. D. Organic Thin Film Transistors Based on *n*-Alkyl Perylene Diimides: Charge Transport Kinetics as a Function of Gate Voltage and Temperature. *Phys. Chem. B* **2004**, *108*, 19281.
23. Tatemichi, S.; Ichikawa, M.; Koyama, T.; Taniguchi, Y. High Mobility *n*-type Thin-Film Tranistors Based on *N*,*N*′-Ditridecyl Perylene Diimide with Thermal Treatments. *Appl. Phys. Lett.* **2006**, *89*, 112108.
24. Langhals, H.; Demmig, S.; Huber, H. Rotational Barriers in Perylene Fluorescent Dyes. *Spectrochim. Acta, Part A* **1988**, *44A*, 1189.
25. Würthner, F.; Thalacker, C.; Diele, S.; Tschierske, C. Fluorescent J-Type Aggregates and Thermotropic Columnar Mesophases of Perylene Bisimide Dyes. *Chem.—Eur. J.* **2001**, *10*, 2245–2253.
26. Würthner, F.; Chen, Z.; Dehm, V.; Stepanenko, V. One-Dimensional Luminescent Nanoaggregates of Perylene Bisimides. *Chem. Commun.* **2006**, *11*, 1188.
27. Hüttner, S.; Sommer, M.; Thelakkat, M. n-Type Organic Field Effect Transistors from Perylene Bisimide Block Copolymers and Homopolymers. *Appl. Phys. Lett.* **2008**, *92*, 093302.
28. Ito, S.; Wehmeier, M.; Brand, J. D.; Kübel, C.; Epsch, R.; Rabe, J. P.; Müllen, K. Synthesis and Self-Assembly of Functionalized Hexa-peri-hexabenzocoronenes. *Chem.—Eur. J.* **2001**, *6*, 4327–4342.
29. Tashiro, K.; Ono, K.; Minagawa, Y.; Kobayashi, M.; Kawai, T.; Yoshino, K. Structure and Thermochromic Solid-State Phase Transition of Poly(3-alkylthiophene). *J. Polym. Sci., Part B* **1991**, *29*, 1223–1233.
30. Sommer, M.; Hüttner, S.; Steiner, U.; Thelakkat, M. Influence of Molecular Weight on the Solar Cell Performance of Double-Crystalline Donor–Acceptor Block Copolymers. *Appl. Phys. Lett.* **2009**, *95*, 83308.
31. Kline, R. J.; McGehee, M. D.; Kadnikova, E. N.; Liu, J.; Fréchet, J. M. J.; Toney, M. F. Dependence of Regioregular Poly(3-hexylthiophene) Film Morphology and Field-Effect Mobility on Molecular Weight. *Macromolecules* **2005**, *38*, 3312–3319.
32. Zen, A.; Saphiannikova, M.; Neher, D.; Grenzer, J.; Grigorian, S.; Pietsch, U.; Asawapirom, U.; Janietz, S.; Scherf, U.; Lieberwirth, I. *et al*. Effect of Molecular Weight on the Structure and Crystallinity of Poly(3-hexylthiophene). *Macromolecules* **2006**, *39*, 2162–2171.
33. Lindner, S.; Kaufmann, N.; Thelakkat, M. Nanostructured Semiconductor Block Copolymers: $\pi-\pi$ Stacking, Optical and Electrochemical Properties. *Org. Electron.* **2007**, *8*, 69–75.
34. Hoffmann, M.; Schmidt, K.; Fritz, T.; Hasche, T.; Agranovich, V.; Leo, K. The Lowest Energy Frenkel and Charge-Transfer Excitons in Quasi-one-dimensional Structures: Application to MePTCDI and PTCDA Crystals. *Chem. Phys.* **2000**, *258*, 73–96.
35. Spano, F. C. J. Modeling Disorder in Polymer Aggregates: The Optical Spectroscopy of Regioregular Poly-(3-hexylthiophene) Thin Films. *Chem. Phys.* **2005**, *122*, 234701.
36. Clark, J.; Silva, C.; Friend, R.; Spano, F. Role of Intermolecular Coupling in the Photophysics of Disordered Organic Semiconductors: Aggregate Emission in Regioregular Polythiophene. *Phys. Rev. Lett.* **2007**, *98*, 206406.
37. Yago, T.; Tamaki, Y.; Furube, A.; Katoh, R. Self-Trapping Limited Exciton Diffusion in a Monomeric Perylene Crystal as Revealed by Femtosecond Transient Absorption Microscopy. *Phys. Chem. Chem. Phys.* **2008**, *10*, 4435–4441.
38. Hüttner, S.; Hodgkiss, J.; Sommer, M.; Friend, R.; Steiner, U.; Thelakkat, M. Charge Dynamics in Donor–Acceptor Block Copolymers Based on Poly(perylene bisimide acrylate) and Poly(thiophene). Unpublished work.
39. Campbell, A.; Hodgkiss, J.; Westenhoff, S.; Howard, I.; Marsh, R.; McNeill, C.; Friend, R.; Greenham, N. Low-Temperature Control of Nanoscale Morphology for High Performance Polymer Photovoltaics. *Nano Lett.* **2008**, *8*, 3942–3947.
40. Westenhoff, S.; Howard, I. A.; Friend, R. H. Probing the Morphology and Energy Landscape of Blends of Conjugated Polymers with sub-10 nm Resolution. *Phys. Rev. Lett.* **2008**, *101*, 016102.
41. Hüttner, S.; Sommer, M.; Chiche, A.; Krausch, G.; Steiner, U.; Thelakkat, M. Controlled Solvent Vapour Annealing for Polymer Electronics. *Soft Matter* **2009**, *5*, 4206–4211.
42. Westenhoff, S.; Howard, I. A.; Hodgkiss, J. M.; Kirov, K. R.; Bronstein, H. A.; Williams, C. K.; Greenham, N. C.; Friend, R. H. Charge Recombination in Organic Photovoltaic Devices with High Open-Circuit Voltages. *J. Am. Chem. Soc.* **2008**, *130*, 13653–13658.
43. Hodgkiss, J.; Tu, G.; Albert-Seifried, S.; Huck, W.; Friend, R. Ion-Induced Formation of Charge-Transfer States in Conjugated Polyelectrolytes. *J. Am. Chem. Soc.* **2009**, *131*, 8913–8921.
44. Laquai, F.; Mishra, A. K.; Müllen, K.; Friend, R. H. Amplified Spontaneous Emission of Poly(ladder-type Phenylene)s—The Influence of Photophysical Properties on ASE Thresholds. *Adv. Funct. Mater.* **2008**, *18*, 3265–3275.